This article is a non-peer reviewed preprint published at EarthArXiv

A New Mechanism for Terrace Formation in Submarine Canyons

Anjali M. Fernandes[1], David Mohrig[1], James Buttles[1],

[1] The Center for Integrative Geoscience, University of Connecticut, Storrs, Connecticut, USA.

[2] The Jackson School of Geosciences, The University of Texas at Austin, Texas, USA.

Email: anjali.fernandes@uconn.edu

Deep canyons on Earth occur in both terrestrial and submarine environments, where they are carved by incising channels. Flights of apparently similar unpaired terraces, seen at the inside of bends in incised sinuous channels, are common in both environments. Here we demonstrate a new mechanism for terrace formation that we believe is unique to settings where sediment transporting flows are only slightly denser than the ambient fluid, such as those encountered in submarine environments or on other planets and moons. Whereas it is well known that variable rates of river incision and lateral migration create bedrock terraces in river canyons, the processes responsible for their submarine counterparts are largely unexplored, limiting our ability to reconstruct canyon evolution and therefore landscape history in these environments. Tangential momentum in turbidity currents traversing canyon bends can cause currents to run far up the outer banks of bends, such that flow separates from inner banks. The result is very little current and very low velocities along the channel bottom near the inside of the bends. We present experimental results that capture terrace formation at the inner banks of bends, through sustained erosion by energetic currents outside low-velocity, flow-separation zones coupled with no erosion or weak deposition within separation zones.

On the Earth's surface, deep canyons (e.g. the Grand Canyon, ~1.83 km deep) present significant erosional relief, and are usually created as a result of river incision into an uplifting and eroding landscape in terrestrial environments; deep submarine canyons (e.g. Zhemchung Canyon, ~2.5 km deep) that dissect Earth's continental margins are also erosional, but incise into a depositional landscape. Although submarine canyons have been the primary conduits for sediment delivery from continental shelves to the deep oceans[1], the erosional mechanics associated with their formation are incompletely understood. Modern and ancient shelf margins contain the record of numerous erosional canyons, carved by turbidity currents and filled in by the deposits of oceanic sediment-transporting flows[2]. Whereas a significant fraction of the morphodynamic history of canyon filling can be assembled by querying the sedimentary record that results[3], elucidating the morphodynamics of canyon erosion is significantly more challenging, as the shape of a canyon represents the composite erosional imprint of numerous geomorphic states. On the modern seafloor, canyons are largely inactive today or challenging to access and instrument[4–7], and so capturing the temporal evolution of these landforms can be a formidable task.

A significant difference between terrestrial and submarine environments is the density of the transporting fluid relative to the density of the ambient fluid. In nature and the laboratory, turbidity currents have been observed to run up the outer walls of channel bends[8,9]. This occurs because the they have densities that are only slightly greater than the ambient water. This phenomenon has been shown to influence depositional patterns in submarine channels, specifically the development of bars at the outer banks of bends [9,10]. For decades, researchers have used physical experiments to study the dynamic interactions between turbidity currents and channels, at reduced spatio-temporal scales[9,11–15]. However, these experiments have focused on either purely depositional turbidity currents or erosional currents that mobilized in-channel sediment as bedload. The non-cohesive sediments used in these experiments possess properties that differ from sediment encountered by canyons incising into shelf margins. The cohesive, compacted or indurated, and generally fine-grained strata on shelf margins can only be entrained when a threshold for particle detachment is exceeded[16]. This “detachment-limited” erosion occurs when the shear stress exerted by the flow overcomes the cohesive strength of the sediment[17], at which point the fine particles are advected down-system into deeper water.

In our experiment we used a channel built of a cohesive mix of fine-grained acrylic sediment (specific gravity = 1.15) and kaolinite clay particles that were easy for laboratory-scale flows to suspend once detached, thereby replicating similar conditions to those encountered in actively eroding, detachment-limited submarine canyons. Specifically, we documented flow and sediment transport patterns associated with terrace formation at the inner banks of bends. Each density current produced net erosion, with detached material almost entirely advected out of the system in suspension (Fig. 2A). In our experiment, the run-up of low excess density currents against the outer walls of channel bends caused the flow to separate from the inner bank of the bend (Fig. 2.B, Fig. 3). Terraces formed within low-velocity flow-separation zones at channel bends. Terrace relief, relative to the lowest point of the channel, grew through accumulation of suspension deposits within the flow separation zone, and sustained erosion outside it along the pathway of the high-velocity core of the current. Flow through the separation zone displayed low sediment concentrations and velocities (~2 cm/s) low enough to permit sedimentation and preclude remobilization of deposited sediment; the highest velocities (>10 cm/s) and sediment concentrations were associated with the main current running up the outside of the bend (Fig. 2; Fig. 3).

Erosion in the channel occurred through wear by abrasion and plucking, evolving the channel bed and outer walls into ornate erosional bedforms in a manner similar that observed in detachment-limited bedrock rivers[17](Fig. 4). Erosional scour pits that initiated at the outer banks of bends grew and propagated downstream, eventually coalescing to form a deeply entrenched inner channel (Fig.1). The leading edges of these pits were sites of high turbulence and focused erosion. They intermittently released clouds of sediment particles that were transported downstream in suspension or aggregates of cohesive sediment that, dragged along by the flow, bounced and scraped along the channel before disintegrating into clouds of suspended sediment. Linear grooves that patterned the channel bed and outer walls of bends, oriented parallel to the direction of flow, were likely formed by the scraping of these aggregates against the bed (Fig. 3), although near-bed turbulence may also have contributed to their formation. Erosion of the channel bed was spatially discontinuous and followed the pathway of the high-velocity core of the current (Fig 1). Enhanced erosion occurred at sites where the channel bed was roughened through plucking or the intersection of linear grooves (Fig. 3).

Strath terraces, etched into bedrock by river incision, have long been recognized as recorders of former river bed elevations. Flights of unpaired terraces along the inner walls of bedrock river meanders, are commonly interpreted to be the result of non-steady lateral erosion or vertical incision rates. Intervals of predominant lateral erosion plane off bedrock terraces which slope gently towards the river channel; intervals of predominant vertical incision form the steep slopes that separate terraces. They sometimes display a thin layer of gravel or coarse bedload, augmented by floodplain deposition. Strath terraces are thought to form through varying rates of river incision or lateral erosion in response to one or more factors such as tectonic uplift, sea-level change, variability in climatically-modulated sediment supply, bedrock strength variability and local channel bed steepening following bend cut-off [18–23].

Terraces near the inner banks of incising submarine channels, similarly thought to record progressive incision and lateral migration, have been documented in a number of submarine channels and canyons[24–27]. We compared the cross-sectional shapes of incisional terrestrial and submarine channels/canyons, at or near their bend apices, to those that were dynamically evolved in our experiment (Fig. 5). To account for their very different scales, we divided local channel depth by the vertical distance between the top of the outer channel wall and the channel thalweg; cross-channel distance was divided by the length equal to the distance between the channel walls at the height of the outerwall. Intriguingly, in all submarine cases a similar percentage of the channel width is occupied by terraces at the insides of bends (50-60%), whereas the terrestrial cases show more variability (30%-70%). Whereas the variability in dimensionless width of inner channels at bend apices in the submarine channels is relatively small (40-50%), the local depth of inner channels compared to total channel relief is quite variable (30-60%). The striking similarities in cross-sectional shapes of natural and experimental incisional submarine channels suggests a degree of self-similarity in the processes that form these features, though the variability in the relative depth of the inner channels is likely due to differences in the incision rate or formation time.

Based on our experimental observations and the dimensionless comparisons, we propose that terraces can form at the insides of bends in submarine canyons when (a) turbidity currents do not fill the cross-sectional area of the canyon and the canyon is wide enough to permit the free meandering of the high velocity core of the current and (b) the outer wall slope is shallow enough to allow run-up of flow at the outside of bends and separation of flow from the inside. The erosional boundary of our experimental terraces coincided with the boundary of the flow separation zones; steep edges separating flights of terraces in natural submarine bends may mark the location of the shifting boundary of the flow separation zone as its shape changed in tandem with the outward erosion of the channel bend through time. Although variable relative rates of incision and lateral migration may, as in bedrock rivers, contribute to the formation of unpaired inner-bank terraces in submarine canyons, terraces may also form through the relatively simple and hitherto under-recognized process of flow separation from the inner bank. In contrast to strath terraces in river canyons, submarine separation-zone terraces will not be capped by bedload deposits, but by suspended load, as bedload transport will track the highest flow velocities and lowest topography towards the outside of the bend.

Furthermore, there can be important differences in the processes that act along the outer walls of canyons: although likely to be subject to hillslope processes in both environments, the outer walls of canyon bends may be significantly modified by turbidity currents at elevations accessible to through-going flows. Canyon walls may even display linear grooves, similar to those seen in our experiment, made by currents running up the outer walls of bends with low slopes. In remotely sensed environments (e.g. the deep ocean, the surfaces of other planets and moons, etc.), the presence of flow-parallel grooves high up on outer canyon walls will likely be diagnostic of extreme flow run-up at the outer walls. Therefore, in order to fully understand the process of canyon evolution, and the landscape history ciphered into canyon morphology, it is important to understand how the eroding flow is partitioned across the channel cross section.

In summary, our results demonstrate that unpaired submarine canyon terraces, though apparently similar in form to those encountered in terrestrial canyons, can be generated by significantly different processes. The formation mechanism of separation-zone terraces require extreme flow run-up at the outer bank and is thus unique to environments in which the eroding currents are only slightly denser than the ambient fluid. We therefore emphasize that the relative density of transporting flows must be taken into account when using canyon morphology to infer formative processes and landscape history in environments on Earth as well as other planets and moons.

Figures & Captions

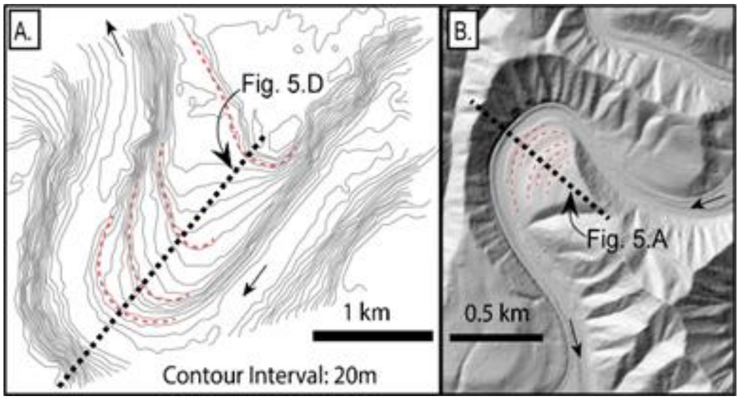

Figure 1: A. Bathymetry map showing unpaired terraces at the inside of a bend in the Congo channel (modified from Babonneau et al., 2010). B. Hillshaded bare earth LiDAR map of a bend in the Smith River, showing flights of unpaired terraces at the inside of the bend.

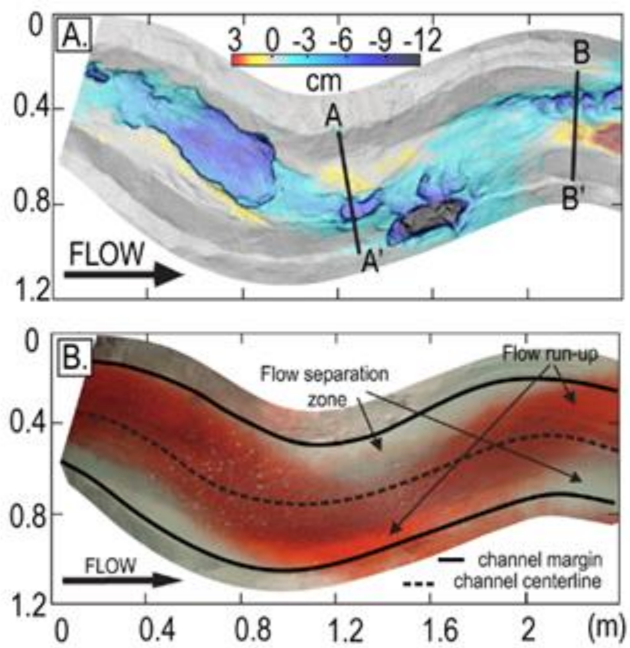

Figure 2: A) A Map of elevation change from the passage of 5 density currents, draped over a slope map of the final channel. B) An overhead photograph showing the passage of a density current (dyed red) through the channel. The high-intensity red dye tracks the path of high velocities, while very little dyed current is apparent within low- velocity flow-separation zones at the inner banks of bends. Terraces in flow-separation zones grew in relief relative to the channel talweg through sustained erosion (cold hues) outside the separation zone and thin suspension deposition (warm hues) within it.

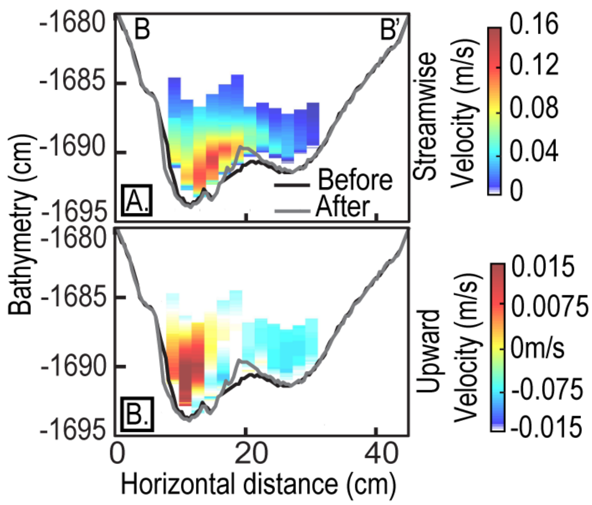

Figure 3: Magnitudes of near-bed velocities, separated into (A) the bed-parallel, downstream component of velocity, and (B) upward directed velocity at cross section B-B' in Fig. 1, collected during the passage of a density current. The surface elevation at B-B' before and after the passage of the density current is shown here. Note the extremely low flow velocities over the terrace, tied to deposition. Upward directed velocities at the outside of the bend in (B) are related to flow run-up and increased turbulence from the rough, eroding bed.

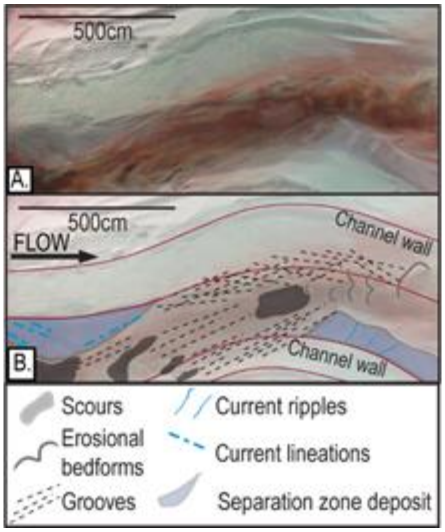

Figure 4: A. Perspective view of the channel bed (through the water column) at the end of the experiment. B. Interpretive overlay indicating surface morphology associated with erosion in the inner channel and deposition on the terraces.

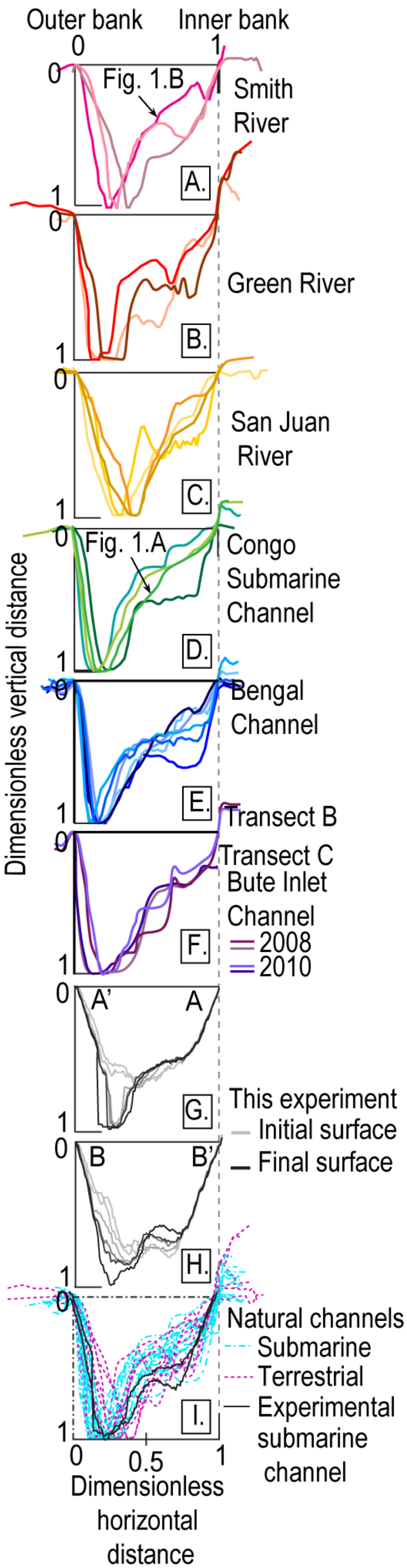

Figure 5: Non-dimensionalized channel cross sections at bend apices in: A) Smith River, Oregon, B) Green River, Utah, C) San Juan River, Utah, D) the Congo submarine channel, Offshore Angola, E) the Bengal submarine channel, Bay of Bengal, F) the Bute submarine channel, British Columbia (from survey years 2008 and 2010), G, H) the submarine channel in our experiment at cross section A-A' and B-B' in Fig. 1A. Note: incision of the inner channel in our experiment was stalled when it reached the concrete platform 5 cm below the sediment bed. I) A comparison of cross-sections through natural and experimental channels in terrestrial and submarine settings show a remarkable similarity in the range of forms encountered at bend apices.

Methods

The experimental basin was 8m long, 6m wide and 2.0m deep. The sinuous channel was built with a weakly cohesive mixture of acrylic particles (specific gravity = 1.15; grain size data in supplementary Information) and clay (volumetric ratio: 10:1) on a sloping concrete ramp in a volumetric ratio of 10:1. The channel form was constructed from the dry sediment mixture and then slowly submerged. The channel was 45 cm wide at the top, 20 cm wide at the base, 14 cm deep and 2.5 m long, with a down-channel slope of approximately 7 degrees and 5 cm of erodible sediment on the channel bed. The channel was built upon a platform separated from the walls of the basin by deep moats that served to prevent currents from reflecting off the tank walls (basin schematic in supplementary information).

Five saline density currents with excess densities ~4% were released into the channel; the last three currents carried a 2% volumetric concentration of suspended acrylic sediment. Density currents were released into an experimental channel through a box with two perforated screens designed to extract momentum from flows. Density currents were ~10 cm thick and did not completely occupy the channel cross section. Saline fluid was not allowed to build-up in the basin during the experiment. Fluid was extracted through the floor drains as it flowed off the raised platform. The water level in the basin was maintained with a constant flux of fresh water and overflow drainage through a weir.

Salt (CaCl2) and water (and sediment, when it was used), were mixed together in a reservoir, until the salt was completely dissolved. The mixture was agitated over several hours and allowed to cool to room temperature (overnight), as the dissolution of this salt in water is an exothermic process. Once at room temperature, the mixture was pumped up to a constant head tank and then allowed to flow into the experimental basin at a controlled rate set by the constant hydraulic head and a system of valves. A generalized cross-section of the experimental basin used is shown in Figure SI1.

High-resolution bathymetry maps (vertical resolution ~100 microns; horizontal resolution = 4 mm), collected before and after each flow define changes wrought through erosion and deposition in the channel. We used a Vectrino Acoustic Doppler Velocimetric Profiler to map the flow field near the channel bed. The near-bed velocities were collected in 1mm vertical bins, and reported velocities were averaged over the time period of each experimental run. Velocity data was averaged Continuous overhead and perspective time-lapse photographs, and video were collected during each experimental run. T channel was photograph after the passage of each current, once sediment in the water column had settled.

References Cited

1. Talling, P. J., Paull, C. K. & Piper, D. J. W. How are subaqueous sediment density flows triggered, what is their internal structure and how does it evolve? Direct observations from monitoring of active flows. *Earth-Sci. Rev.* **125,** 244–287 (2013).
2. Wynn, R. B., Cronin, B. T. & Peakall, J. Sinuous deep-water channels: Genesis, geometry and architecture. *Mar. Pet. Geol.* **24,** 341–387 (2007).
3. Deptuck, M. E., Sylvester, Z., Pirmez, C. & O'Byrne, C. Migration–aggradation history and 3-D seismic geomorphology of submarine channels in the Pleistocene Benin-major Canyon, western Niger Delta slope. *Mar. Pet. Geol.* **24,** 406–433 (2007).
4. Symons, W. O. *et al.* A new model for turbidity current behavior based on integration of flow monitoring and precision coring in a submarine canyon. *Geology* **45,** 367–370 (2017).
5. Azpiroz-Zabala, M. *et al.* Newly recognized turbidity current structure can explain prolonged flushing of submarine canyons. *Sci Adv* **3,** e1700200 (2017).
6. Hughes Clarke, J. E. First wide-angle view of channelized turbidity currents links migrating cyclic steps to flow characteristics. *Nat. Commun.* **7,** 11896 (2016).
7. Khripounoff, A. *et al.* Direct observation of intense turbidity current activity in the Zaire submarine valley at 4000 m water depth. *Mar. Geol.* **194,** 151–158 (2003).
8. Hay, A. E. Turbidity currents and submarine channel formation in Rupert Inlet, British Columbia: 1. Surge observations. *J. Geophys. Res.* **92,** 2875–2881 (1987).
9. Straub, K. M., Mohrig, D., McElroy, B. & Buttles, J. Interactions between turbidity currents and topography in aggrading sinuous submarine channels: A laboratory study. *Geological Society of America Bulletin* (2008).
10. Nakajima, T., Peakall, J., McCaffrey, W. D., Paton, D. A. & Thompson, P. J. P. Outer-Bank Bars: A New Intra-Channel Architectural Element within Sinuous Submarine Slope Channels. *J. Sediment. Res.* **79,** 872–886 (2009).

11. Métivier, F., Lajeunesse, E. & Cacas, M.-C. Submarine Canyons in the Bathtub. *J. Sediment. Res.* **75,** 6–11 (2005).
12. Mohrig, D. & Buttles, J. Deep turbidity currents in shallow channels. *Geology* **35,** 155–158 (2007).
13. Amos, K. J. *et al.* The influence of bend amplitude and planform morphology on flow and sedimentation in submarine channels. *Mar. Pet. Geol.* **27,** 1431–1447 (2010).
14. Janocko, M., Cartigny, M. B. J., Nemec, W. & Hansen, E. W. M. Turbidity current hydraulics and sediment deposition in erodible sinuous channels: Laboratory experiments and numerical simulations. *Mar. Pet. Geol.* **41,** 222–249 (2013).
15. de Leeuw, J., Eggenhuisen, J. T. & Cartigny, M. J. B. Morphodynamics of submarine channel inception revealed by new experimental approach. *Nat. Commun.* **7,** 10886 (2016).
16. Mitchell, N. C. Bedrock erosion by sedimentary flows in submarine canyons. *Geosphere* **10,** 892–904 (2014).
17. Whipple, K. X. Bedrock Rivers and the Geomorphology of Active Orogens. *Annu. Rev. Earth Planet. Sci.* **32,** 151–185 (2004).
18. Davis, W. M. The terraces of the Westfield River, Massachusetts. *Am. J. Sci.* **Series 414,** 77–94 (1902).
19. Pazzaglia, F. J. & Gardner, T. W. Fluvial terraces of the lower Susquehanna River. *Geomorphology* **8,** 83–113 (1993).
20. Hancock, G. S. & Anderson, R. S. Numerical modeling of fluvial strath-terrace formation in response to oscillating climate. *GSA Bulletin* **114,** 1131–1142 (2002).
21. Stark, C. P. *et al.* The climatic signature of incised river meanders. *Science* **327,** 1497–1501 (2010).
22. Finnegan, N. J. & Dietrich, W. E. Episodic bedrock strath terrace formation due to meander migration and cutoff. *Geology* **39,** 143–146 (2011).
23. Limaye, A. B. S. & Lamb, M. P. Numerical simulations of bedrock valley evolution by

meandering rivers with variable bank material. *Journal of Geophysical Research: Earth Surface* **119,** 927–950 (2014).

24. Shepard, F. P. Meander in valley crossing a deep-ocean fan. *Science* **154,** 385–386 (1966).
25. Babonneau, N., Savoye, B., Cremer, M. & Bez, M. Sedimentary Architecture in Meanders of a Submarine Channel: Detailed Study of the Present Congo Turbidite Channel (Zaiango Project). *J. Sediment. Res.* **80,** 852–866 (2010).
26. Conway, K. W., Barrie, J. V., Picard, K. & Bornhold, B. D. Submarine channel evolution: active channels in fjords, British Columbia, Canada. *Geo-Mar. Lett.* **32,** 301–312 (2012).
27. Maier, K. L. *et al.* Punctuated Deep-Water Channel Migration: High-Resolution Subsurface Data from the Lucia Chica Channel System, Offshore California, U.S.A. *J. Sediment. Res.* **82,** 1–8 (2012).

Acknowledgements

For financial support, the authors acknowledge the Jackson School of Geosciences, the CSM-UT RioMAR Industry Consortium for financial support of this work, and The Oregon Department of Geology and Mineral Industries for the LiDAR data used in Fig 1..

Author Contributions

A.M.F. conducted the experiments, compiled and analyzed data and was the lead author of the manuscript; D.M. provided significant editorial feed-back on the manuscript; J.B. assisted with experiments and data analyses and provided significant editorial feed-back on the manuscript.

Competing Financial Interests

The authors declare no competing financial interests.

Supplementary Information

Experiment Design

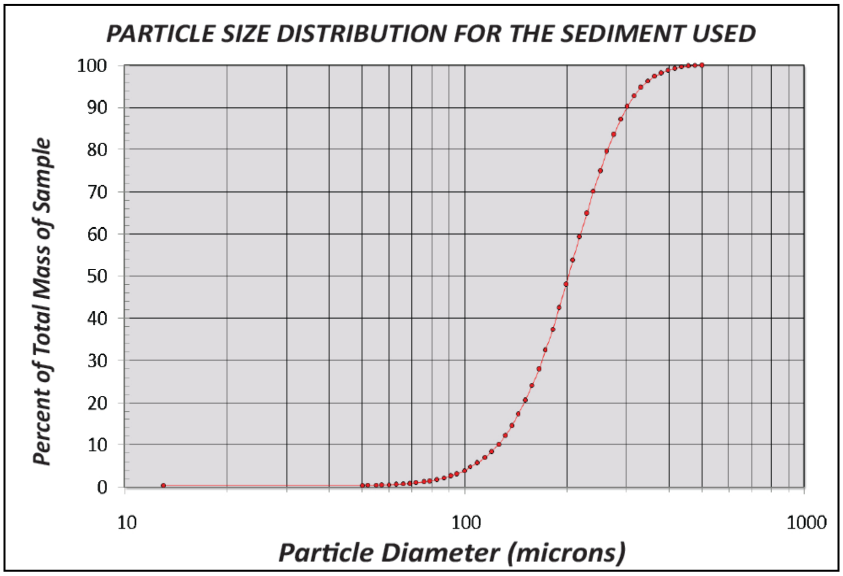

Figure SI-1: The grain-size distribution of acrylic sediment used.

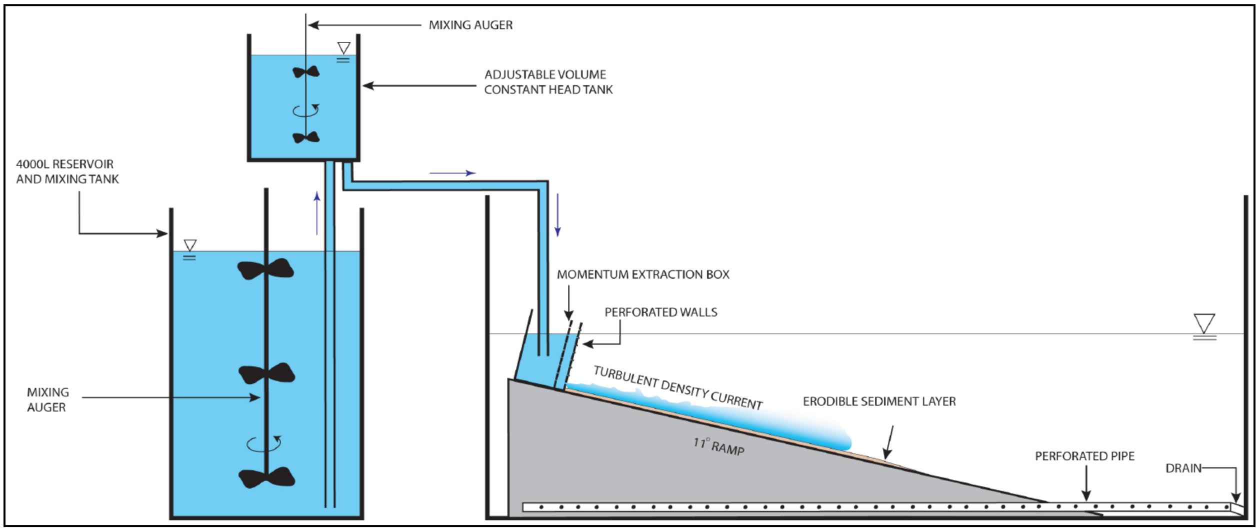

Figure SI-2: A generalized schematic of the experimental basin

Dynamic Scaling

This laboratory experiment can be roughly compared to natural systems through the scaling of three dimensionless variables, the densimetric Froude number (Frd), the Reynolds number (Re) and the ratio of particle fall velocity (ws) to current shear velocity (u*). An approximate dynamic similarity was assumed by setting Frd (lab) = Frd (prototype) [1]. Resulting prototype values of depth-averaged velocity, current thickness and flow duration are compiled in DR Table 1. Sediment transport properties are compared between experimental and natural systems by setting the ratio ws/u*(lab) equal to ws/u*(prototype). Values for ws were computed using the empirically derived relationship of ([2]). Shear velocities (u*) for the experimental currents were estimated as u*=(uCd)^½ where u is the depth averaged velocity of the density currents and Cd is the hydraulic drag coefficient approximated by the value 0.02 for experimental channels and 0.002 for natural channels[3,4]. Note: shear velocities estimated thus are greater than 3 times the estimated settling velocity of the D99 of acrylic particles used, indicating that particles were fully suspended once detached from the bed [5]. This quantitatively agrees with visual observations of transport patterns. Geometric and dynamic properties of the channels and currents, scaled approximately to natural systems, is shown in Table SI-1.

Table SI-1: Geometries and dynamics of experimental channel scaled to natural systems

		Experiment	Prototype
Geometric Scaling	channel depth	0.15m	50m
	channel width	0.50m	500m

Dynamic Scaling	depth averaged velocity	0.10m/s	1.83m/s
	shear velocity	0.045m/s	0.060m/s
	Fr d	0.41	0.41
	Re	15000	6 x 107
	Sediment composition and grain-size distribution (micron)	Acrylic D1=49 , D10=88 , D25=127, D50=146, D75=205, D90=243, D99=340	Quartz. D1=19 , D10=33 , D25=47, D50=55, D75=75, D90=89, D99=124
	flow duration	25min	40-72 minutes
	current thickness	~0.10m	33m

Topographic data

Table SI-2: Data sources / locations for Figure 5

	Terrestrial Channels	Coordinates of end points of cross-section	Source
1	Smith River1	-123.7826371901627,43.80472633714489; -123.7746010278586,43.79981995552907	Oregon Department of Geology and Mineral Industries
2	Smith River2	-123.7604201127893,43.81115517323132; -123.7673292848834,43.79830226749066	
3	Smith River3	-123.6532970276423,43.81939479072555; -123.6600247308344,43.8065667856463	
4	Green River1	-109.6388033169158,38.58624113046864; -109.6419008067904,38.56505600805119	Google Earth
5	Green River2	-110.0523449828799,38.65642315320836; -110.0565156794953,38.63796866905698	Google Earth
6	Green River3	-109.8010734570593,38.31466238795997; -109.7542006529873,38.30187390633612	Google Earth
7	Green River4	-110.0856706426976,38.65581941640971; -110.0639219942443,38.6803400020592	Google Earth
8	Colorado River	-110.908639822533,37.36145671781638; -110.8423561906744,37.33219665078475	Google Earth
9	San Juan River1	-109.7738676542044,37.21584872989421; -109.7526641747123,37.18948841812345	Google Earth
10	San Juan River2	-109.9189523741587,37.16557981421435; -109.9270346290523,37.1540908316806	Google Earth
11	San Juan River3	-109.7314943800335,37.20198777373232; -109.7401657271749,37.18926444104969	Google Earth

12	San Juan River4	-109.7763911352864,37.1900553535192; -109.7565150459447,37.18227160590539	Google Earth
	Submarine Channels	Source	
13	Congo Channel1-4	Babonneau et al., 2010[6] (Fig. 4, inset 1; Fig. 5 cross-sections; Fig. 7 cross-section	
17	Bengal Channel1-6	Data provided by Tilmann Schwenk[7,8]. See data below.	
19	Bute Inlet Channel1-2	Conway et al., 2013,[9] Fig. 6b	

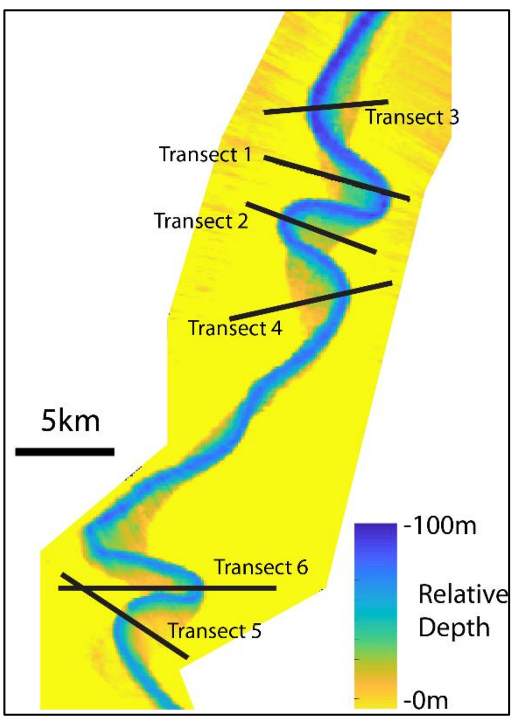

Figure SI-3: Topographic data from the Bengal Channel

Table SI-3: Bengal Channel cross sections used in Fig.5E

X	Y	Z
Transect 1		
3561.814	2764.549	499.4587
3562.088	2765.511	500.2395
3562.363	2766.472	500.2395
3562.638	2767.434	502.1104
3562.913	2768.395	502.0762
3563.187	2769.357	501.0259
3563.462	2770.319	499.7043
3563.737	2771.28	499.2727
3564.011	2772.242	500.728
3564.286	2773.203	501.323
3564.561	2774.165	501.2463
3564.836	2775.126	501.6074
3565.11	2776.088	501.7815
3565.385	2777.049	501.3899

3565.66	2778.011	501.7163
3565.935	2778.972	503.8127
3566.209	2779.934	505.8171
3566.484	2780.895	505.4263
3566.759	2781.857	505.1541
3567.033	2782.818	505.019
3567.308	2783.78	506.4709
3567.583	2784.741	503.582
3567.858	2785.703	496.9043
3568.132	2786.664	487.2913
3568.407	2787.626	482.1067
3568.682	2788.587	484.4988
3568.956	2789.549	484.1414
3569.231	2790.511	485.6184
3569.506	2791.472	484.3679
3569.781	2792.434	485.4331
3570.055	2793.395	484.0623
3570.33	2794.357	478.2397

3570.605	2795.318	478.0498
3570.879	2796.28	470.3757
3571.154	2797.241	466.5708
3571.429	2798.203	461.1531
3571.704	2799.164	460.3745
3571.978	2800.126	461.6633
3572.253	2801.087	460.79
3572.528	2802.049	461.573
3572.803	2803.01	461.2161
3573.077	2803.972	459.4604
3573.352	2804.933	455.8821
3573.627	2805.895	455.2827
3573.901	2806.856	451.5835
3574.176	2807.818	445.7292
3574.451	2808.779	438.8989
3574.726	2809.741	438.0415
3575	2810.703	435.6125
3575.275	2811.664	430.3228

3575.55	2812.626	424.4956
3575.824	2813.587	421.238
3576.099	2814.549	419.8865
3576.374	2815.51	419.7874
3576.649	2816.472	419.0134
3576.923	2817.433	422.1704
3577.198	2818.395	433.8303
3577.473	2819.356	460.5615
3577.748	2820.318	486.6248
3578.022	2821.279	501.8035
3578.297	2822.241	502.1074
3578.572	2823.202	499.9741
3578.846	2824.164	499.4375
3579.121	2825.125	498.3967
3579.396	2826.087	496.7734
3579.671	2827.048	498.1201
Transect 2		
3580.808	2750.553	505.0867

3581.156	2751.491	505.0867
3581.504	2752.428	503.8159
3581.852	2753.366	504.9336
3582.2	2754.303	505.1396
3582.547	2755.241	501.9661
3582.895	2756.179	502.2168
3583.243	2757.116	502.7256
3583.591	2758.054	500.7629
3583.939	2758.991	501.7971
3584.287	2759.929	506.5491
3584.634	2760.866	502.5356
3584.982	2761.804	503.3899
3585.33	2762.742	504.6633
3585.678	2763.679	504.491
3586.026	2764.617	506.3777
3586.373	2765.554	499.7292
3586.721	2766.492	494.3931
3587.069	2767.429	469.8796

3587.417	2768.367	442.479
3587.765	2769.305	418.8752
3588.112	2770.242	417.1028
3588.46	2771.18	421.863
3588.808	2772.117	432.7422
3589.156	2773.055	438.373
3589.504	2773.992	446.8213
3589.851	2774.93	453.7612
3590.199	2775.868	457.0576
3590.547	2776.805	459.9719
3590.895	2777.743	457.7002
3591.243	2778.68	459.8496
3591.59	2779.618	465.2078
3591.938	2780.555	467.7456
3592.286	2781.493	467.7456
3592.634	2782.43	468.8381
3592.982	2783.368	470.0203
3593.33	2784.306	468.5266

3593.677	2785.243	466.949
3594.025	2786.181	468.2185
3594.373	2787.118	468.8608
3594.721	2788.056	465.8953
3595.069	2788.993	470.0505
3595.416	2789.931	470.6814
3595.764	2790.869	469.5479
3596.112	2791.806	470.1123
3596.46	2792.744	468.7937
3596.808	2793.681	468.5659
3597.155	2794.619	471.7056
3597.503	2795.556	480.1018
3597.851	2796.494	480.1018
3598.199	2797.432	489.9429
3598.547	2798.369	506.3
3598.894	2799.307	506.0481
3599.242	2800.244	506.9702
3599.59	2801.182	506.2085

3599.938	2802.119	506.8308
3600.286	2803.057	507.4011
3600.633	2803.995	502.7939
3600.981	2804.932	503.9058
3601.329	2805.87	504.3345
3601.677	2806.807	500.1052
3602.025	2807.745	500.7297
3602.372	2808.682	501.4092
3602.72	2809.62	499.7183
3603.068	2810.557	498.989
3603.416	2811.495	498.989
3603.764	2812.433	499.907
Transect 3		
3538.154	2758.884	492.3789
3538.086	2759.882	493.3291
3538.018	2760.88	494.3196
3537.951	2761.877	494.7246
3537.883	2762.875	496.821

3537.815	2763.873	500.634
3537.748	2764.871	500.0891
3537.68	2765.868	498.2144
3537.612	2766.866	498.6411
3537.545	2767.864	499.9253
3537.477	2768.861	496.3804
3537.41	2769.859	496.0671
3537.342	2770.857	495.2263
3537.274	2771.854	495.3469
3537.207	2772.852	496.3381
3537.139	2773.85	496.2793
3537.071	2774.848	494.5564
3537.004	2775.845	495.2874
3536.936	2776.843	498.782
3536.868	2777.841	500.0381
3536.801	2778.838	489.6682
3536.733	2779.836	463.3796
3536.665	2780.834	433.0459

3536.598	2781.832	416.0168
3536.53	2782.829	413.8276
3536.463	2783.827	414.3398
3536.395	2784.825	417.0977
3536.327	2785.822	422.9158
3536.26	2786.82	429.2554
3536.192	2787.818	434.5452
3536.124	2788.816	440.3308
3536.057	2789.813	444.801
3535.989	2790.811	448.0361
3535.921	2791.809	452.8691
3535.854	2792.806	458.342
3535.786	2793.804	465.0117
3535.718	2794.802	467.2815
3535.651	2795.8	466.825
3535.583	2796.797	472.5129
3535.516	2797.795	477.3623
3535.448	2798.793	480.0486

3535.38	2799.79	482.4045
3535.313	2800.788	483.4497
3535.245	2801.786	480.4539
3535.177	2802.783	482.0789
3535.11	2803.781	486.8608
3535.042	2804.779	493.8394
3534.974	2805.777	498.7195
3534.907	2806.774	501.8169
3534.839	2807.772	498.8428
3534.771	2808.77	497.7661
3534.704	2809.767	497.9216
3534.636	2810.765	496.7517
3534.569	2811.763	498.2197
3534.501	2812.761	498.7166
3534.433	2813.758	497.5544
3534.366	2814.756	498.1433
3534.298	2815.754	497.1812
3534.23	2816.751	497.1885

3534.163	2817.749	496.7751
Transect 4		
3635.46	2743.222	509.8472
3635.238	2744.197	511.429
3635.015	2745.172	511.2734
3634.793	2746.147	510.5366
3634.571	2747.122	509.3396
3634.348	2748.097	509.5215
3634.126	2749.072	509.6775
3633.904	2750.047	510.7617
3633.681	2751.022	513.7332
3633.459	2751.997	508.2424
3633.236	2752.972	508.3435
3633.014	2753.947	507.8877
3632.792	2754.921	507.0134
3632.569	2755.896	508.3696
3632.347	2756.871	508.5454
3632.125	2757.846	506.4949

3631.902	2758.821	506.2175
3631.68	2759.796	507.4346
3631.458	2760.771	508.2148
3631.235	2761.746	510.0637
3631.013	2762.721	508.5295
3630.79	2763.696	504.9785
3630.568	2764.671	506.6875
3630.346	2765.646	509.3352
3630.123	2766.621	507.4846
3629.901	2767.596	506.5371
3629.679	2768.571	509.0146
3629.456	2769.546	508.5427
3629.234	2770.521	509.2092
3629.012	2771.496	509.2092
3628.789	2772.471	506.7678
3628.567	2773.446	500.9426
3628.345	2774.421	494.6709
3628.122	2775.396	491.1914

3627.9	2776.371	490.79
3627.677	2777.346	490.759
3627.455	2778.321	487.0527
3627.233	2779.296	483.4392
3627.01	2780.271	480.6494
3626.788	2781.246	480.436
3626.566	2782.22	478.9146
3626.343	2783.195	476.7307
3626.121	2784.17	474.1692
3625.899	2785.145	472.187
3625.676	2786.12	470.781
3625.454	2787.095	475.3787
3625.231	2788.07	475.4653
3625.009	2789.045	472.719
3624.787	2790.02	471.9294
3624.564	2790.995	468.7434
3624.342	2791.97	463.4287
3624.12	2792.945	456.6833

3623.897	2793.92	446.4316
3623.675	2794.895	434.4077
3623.453	2795.87	427.3394
3623.23	2796.845	425.7461
3623.008	2797.82	429.23
3622.786	2798.795	446.6494
3622.563	2799.77	472.7124
3622.341	2800.745	492.1047
3622.118	2801.72	506.2705
3621.896	2802.695	510.2144
3621.674	2803.67	506.2119
3621.451	2804.645	503.2959
3621.229	2805.62	503.0471
3621.007	2806.595	503.562
3620.784	2807.57	504.9954
3620.562	2808.545	505.6348
3620.34	2809.52	506.8853
3620.117	2810.494	506.8853

3619.895	2811.469	504.8274
3619.672	2812.444	502.2617
3619.45	2813.419	501.7261
3619.228	2814.394	500.897
3619.005	2815.369	499.498
3618.783	2816.344	498.7126
3618.561	2817.319	498.3611
3618.338	2818.294	494.4478
Transect 5		
3761.092	2664.244	510.0837
3761.082	2665.244	509.9277
3761.072	2666.244	511.0129
3761.063	2667.244	507.6892
3761.053	2668.244	509.8535
3761.043	2669.244	513.2371
3761.033	2670.243	517.2832
3761.023	2671.243	517.1162
3761.013	2672.243	517.8604

3761.003	2673.243	519.4021
3760.993	2674.243	519.5408
3760.984	2675.243	521.2952
3760.974	2676.243	521.4998
3760.964	2677.243	522.3289
3760.954	2678.243	523.9277
3760.944	2679.243	522.2039
3760.934	2680.243	522.1843
3760.924	2681.243	524.8862
3760.914	2682.243	526.2283
3760.905	2683.243	525.4902
3760.895	2684.243	523.3333
3760.885	2685.243	522.9604
3760.875	2686.243	523.6992
3760.865	2687.243	523.7522
3760.855	2688.243	523.8733
3760.845	2689.243	524.6152
3760.836	2690.243	526.0134

3760.826	2691.242	528.0356
3760.816	2692.242	530.1946
3760.806	2693.242	530.7839
3760.796	2694.242	529.1428
3760.786	2695.242	530.2722
3760.776	2696.242	533.3503
3760.766	2697.242	529.6538
3760.757	2698.242	518.0305
3760.747	2699.242	503.6838
3760.737	2700.242	494.1946
3760.727	2701.242	491.074
3760.717	2702.242	490.0942
3760.707	2703.242	490.2227
3760.697	2704.242	489.6548
3760.688	2705.242	487.3076
3760.678	2706.242	487.3772
3760.668	2707.242	486.3489
3760.658	2708.242	485.1738

3760.648	2709.242	485.0693
3760.638	2710.242	485.7356
3760.628	2711.241	483.345
3760.618	2712.241	484.228
3760.609	2713.241	484.5107
3760.599	2714.241	482.6208
3760.589	2715.241	479.9851
3760.579	2716.241	480.4297
3760.569	2717.241	478.333
3760.559	2718.241	476.2656
3760.549	2719.241	474.3916
3760.54	2720.241	475.2432
3760.53	2721.241	474.114
3760.52	2722.241	470.0115
3760.51	2723.241	466.0439
3760.5	2724.241	461.783
3760.49	2725.241	457.0117
3760.48	2726.241	453.0073

3760.47	2727.241	449.2708
3760.461	2728.241	439.688
3760.451	2729.241	429.9866
3760.441	2730.241	427.614
3760.431	2731.241	446.1775
3760.421	2732.24	486.0601
3760.411	2733.24	514.52
3760.401	2734.24	519.6113
3760.391	2735.24	518.8157
3760.382	2736.24	519.6465
3760.372	2737.24	519.6323
3760.362	2738.24	517.5796
3760.352	2739.24	518.0757
3760.342	2740.24	519.5083
3760.332	2741.24	518.7087
3760.322	2742.24	518.4229
3760.313	2743.24	519.9045
3760.303	2744.24	522.5981

3760.293	2745.24	524.2671
3760.283	2746.24	523.5745
3760.273	2747.24	521.5813
3760.263	2748.24	517.8965
3760.253	2749.24	513.0854
3760.243	2750.24	515.3662
3760.234	2751.24	517.978
3760.224	2752.239	518.75
3760.214	2753.239	515.8105
3760.204	2754.239	518.3206
3760.194	2755.239	521.0134
3760.184	2756.239	519.2241
3760.174	2757.239	517.5723
3760.165	2758.239	518.324
3760.155	2759.239	516.5085
3760.145	2760.239	514.6724
3760.135	2761.239	516.0088
3760.125	2762.239	515.4097

3760.115	2763.239	512.7402
3760.105	2764.239	514.2402
3760.095	2765.239	516.7664
Transect 6		
3793.083	2724.894	531.3044
3792.543	2724.052	532.7021
3792.002	2723.211	532.8149
3791.462	2722.37	531.7319
3790.921	2721.528	531.7319
3790.381	2720.687	533.0977
3789.84	2719.846	531.6421
3789.3	2719.004	532.5063
3788.759	2718.163	533.1738
3788.219	2717.322	531.2031
3787.678	2716.48	520.9128
3787.138	2715.639	509.6631
3786.597	2714.798	498.251
3786.057	2713.956	491.5867

3785.516	2713.115	489.1787
3784.975	2712.274	488.7603
3784.435	2711.432	487.9541
3783.894	2710.591	487.9541
3783.354	2709.75	488.8
3782.813	2708.908	490.8989
3782.273	2708.067	491.5117
3781.732	2707.226	493.5405
3781.192	2706.384	494.5083
3780.651	2705.543	494.5083
3780.111	2704.702	494.3167
3779.57	2703.86	494.7908
3779.03	2703.019	495.5085
3778.489	2702.178	489.1948
3777.949	2701.336	483.4529
3777.408	2700.495	477.3682
3776.868	2699.654	477.3682
3776.327	2698.812	471.3027

3775.787	2697.971	466.5161
3775.246	2697.13	461.7769
3774.706	2696.288	457.708
3774.165	2695.447	458.0515
3773.625	2694.606	458.0515
3773.084	2693.764	466.7202
3772.544	2692.923	470.5908
3772.003	2692.082	503.4775
3771.462	2691.24	530.6262
3770.922	2690.399	535.4709
3770.381	2689.558	532.7119
3769.841	2688.716	527.9897
3769.3	2687.875	528.2622
3768.76	2687.034	530.4871
3768.219	2686.192	531.8411
3767.679	2685.351	529.2329
3767.138	2684.51	529.1648
3766.598	2683.668	526.8899

3766.057	2682.827	527.0752
3765.517	2681.986	526.438
3764.976	2681.144	525.1165
3764.436	2680.303	522.7183
3763.895	2679.462	522.574
3763.355	2678.62	521.6746
3762.814	2677.779	520.2239
3762.274	2676.938	521.7698
3761.733	2676.096	521.3103
3761.193	2675.255	521.2952
3760.652	2674.414	519.5408
3760.112	2673.572	519.9771
3759.571	2672.731	518.1797
3759.031	2671.89	518.3035
3758.49	2671.048	518.2732
3757.949	2670.207	516.6565
3757.409	2669.366	515.6716
3756.868	2668.525	515.6716

3756.328	2667.683	516.7539
3755.787	2666.842	515.3152
3755.247	2666.001	511.0154

References cited

1. Graf, W. H. Hydraulics of sediment transport, Series in water resources and environmental engineering. (1971).
2. Dietrich, W. E. Settling velocity of natural particles. *Water Resour. Res.* **18,** 1615–1626 (1982).
3. Parker, G., Garcia, M., Fukushima, Y. & Yu, W. Experiments on turbidity currents over an erodible bed. *J. Hydraul. Res.* **25,** 123–147 (1987).
4. Garcia Marcelo H. Depositional Turbidity Currents Laden with Poorly Sorted Sediment. *J. Hydraul. Eng.* **120,** 1240–1263 (1994).
5. Smith, J. D. & Hopkins, T. S. *Sediment Transport on the Continental Shelf Off Washington and Oregon in Light of Recent Current Measurements*. (Washington Univ., Seattle. Dept. of Oceanography. Atomic Energy Commission, Athens (Greece), 1971).
6. Babonneau, N., Savoye, B., Cremer, M. & Bez, M. Sedimentary Architecture in Meanders of a Submarine Channel: Detailed Study of the Present Congo Turbidite Channel (Zaiango Project). *J. Sediment. Res.* **80,** 852–866 (2010).
7. Schwenk, T., Speiß, V., Hübscher, C. & Breitzke, M. Frequent channel avulsions within the active channel--levee system of the middle Bengal Fan—an exceptional channel--levee development derived from Parasound and Hydrosweep data: Deep-Sea Research II, v. 50. *Deep-Sea Res.* **50,** 1023–1045 (2003).

8. Schwenk, T., Spiess, V., Breitzke, M. & Huebscher, C. The architecture and evolution of the Middle Bengal Fan in vicinity of the active channel–levee system imaged by high-resolution seismic data. **22,** 637–656 (2005).
9. Conway, K. W., Barrie, J. V., Picard, K. & Bornhold, B. D. Submarine channel evolution: active channels in fjords, British Columbia, Canada. *Geo-Mar. Lett.* **32,** 301–312 (2012).